HHS Public Access

Author manuscript

PET Clin. Author manuscript; available in PMC 2018 February 05.

Published in final edited form as:

PET Clin. 2016 April ; 11(2): 129–149. doi:10.1016/j.cpet.2015.10.002.

Magnetic resonance imaging-guided attenuation correction of positron emission tomography data in PET/MRI

David Izquierdo-Garcia and **Ciprian Catana**

Athinoula A. Martinos Center for Biomedical Imaging, Department of Radiology, Massachusetts General Hospital and Harvard Medical School, Charlestown, Massachusetts

Synopsis

Attenuation correction (AC) is one of the most important challenges in the recently introduced combined positron emission tomography/magnetic resonance imaging (PET/MR) scanners. PET/MR AC (MR-AC) approaches aim to develop methods that allow accurate estimation of the linear attenuation coefficients (LACs) of the tissues and other components located in the PET field of view (FoV). MR-AC methods can be divided into three main categories: segmentation-, atlas- and PET-based. This review aims to provide a comprehensive list of the state of the art MR-AC approaches as well as their pros and cons. The main sources of artifacts such as body-truncation, metallic implants and hardware correction will be presented. Finally, this review will discuss the current status of MR-AC approaches for clinical applications.

Keywords

PET/MRI; Attenuation Correction; MR-AC; segmentation; atlas; template; artifacts; body truncation; implants

Introduction

Attenuation correction (AC) is one of the most important corrections that need to be performed in PET imaging (Fig. 1) AC methods aim to account for the photon attenuation along each line of response (LOR). For this purpose, maps of the linear attenuation coefficients (LACs) for all the tissues and materials located in the PET field of view are generated or integrals of these values along all the LORs are directly measured. As the procedure for including this information in the reconstruction (i.e. performing the actual correction) is similar no matter how these values are obtained, from here on we will refer to the various attenuation map estimation techniques discussed as AC methods. Recently, in parallel with the development of combined PET/MRI scanners, a new class of methods that use the MR information AC (MR-AC) has emerged. This is not a trivial task because the MR signal is related to proton density and tissue relaxation times while photon attenuation is linked to the electron density of the body tissues. The growing interest in this research field is reflected by the increasing number of publications reporting novel methods or comparisons between the different approaches (Fig. 2). However, we should note that even

The authors declare no conflict of interest.

in integrated PET/MRI scanners, the PET data could also be used to derive LACs (PET-AC methods) with or without using external devices such as transmission sources (Tx-based methods).

This review aims to highlight the state-of-the-art methods for MR-AC. Our goal was not to provide full methodological details (see (1, 2) for this purpose), but rather to guide the reader through the available alternatives and briefly present their pros and cons. Additionally, we will discuss those methods that have been proposed for addressing more specific challenges, such as artifacts related to metallic implants, body truncation, and MR hardware. Finally, we will discuss the latest comparative and clinical studies in which different MR-AC methods have been quantitatively and qualitatively evaluated.

MR-AC: AC methods for PET/MRI

Although AC was already known and applied in PET since the early days, the systematic study of AC methods and their effects on PET image quantification started in 1979 with the publication by Huang, Hoffman, Phelps and Kuhl on the “Effects of Inaccurate Attenuation Correction”, as part of a series of studies on PET image quantification (3). This was the first publication investigating the effects on PET image quantification of inaccurate calculation of the attenuation correction factors (ACFs), the mismatch between emission and transmission and of the noise in ACFs estimation, among others. Since then, several studies have tried to identify solutions to such challenges or to minimize (or eliminate) the need for the time-costly transmission scans (4, 5). More than 35 years later, we are facing similar challenges with a newer technology, PET/MRI, such as the need to reduce the errors of MR-AC methods and to minimize the time-consuming data collection required for these approaches (i.e. long MR acquisition times).

Most of the developed MR-AC methods have focused on brain and only a handful have been applied to whole-body imaging. This is due to the fact that whole-body AC poses more challenges that are more difficult to address appropriately than head AC: higher inter-subject anatomical variability, large intra- and inter-subject lung-density (and therefore attenuation properties) variability, non-rigid motion either due to physiological (respiratory and cardiac) or non-physiological (voluntary) movements, body truncation artifacts, routine use of flexible RF coils, difficulty in obtaining MR signal from bone, etc. Because of their scarcity, within this review, methods that apply to whole-body will be explicitly highlighted in **bold** for an easier identification.

Currently, there are only three Food and Drug Administration (FDA) approved methods for AC in combined PET/MRI: a 3-class (air, soft-tissue and lung) segmentation-based method implemented in the sequential Philips PET/MR scanner (6, 7) and two 4-class (air, fat, soft-tissue and lungs) segmentation-based method implemented in the simultaneous Siemens Biograph mMR scanner that was based on the work of Martinez-Moller et al. (8) and in the new simultaneous time-of-flight (ToF) PET/MR from GE (Signa PET/MR) for whole-body imaging (9). None of them properly accounts for bone tissue attenuation, which has been shown to produce large PET image bias (Fig. 3). Additionally, the GE approach also uses an atlas approach for head AC that does include bone tissue as a separate class. A myriad of

MR-AC methods have recently been proposed and compared to the commercially available ones. We can group these methods in three main categories: two MR-based: segmentation- and atlas-based methods and one emission-based (PET-AC) that includes joint estimation, emission-based only methods and transmission-based approaches (Tx-AC).

Segmentation-based methods

Rationale—Segmentation-based methods rely on the accurate segmentation (classification) of MR images into separate attenuating tissue classes. Once segmented, a unique LAC is assigned to each tissue class. The segmentation/classification step is critical to obtain optimal results, in addition to the appropriate choice of the LAC for each tissue class. While we intentionally did not discuss here the effect of the LAC choice, this issue has been addressed in other reviews (e.g. see references (1) and (2)).

Challenges, Pros and Cons—The main challenges for MR-based segmentation-based methods are twofold. First, the accurate and robust segmentation of various tissue classes becomes even more challenging in the case of MR because the lack of absolute quantification of the MRI signal makes the translation of the algorithms more difficult and the non-homogeneity of the main magnetic field leads to image intensity bias. Second, the small (and often null) signal obtained with standard MR sequences from bone tissues due to its very rapid T2* relaxation times complicates its segmentation from the air cavities (also with very low or null MR signal). Accurate air and bone segmentation is critical since they are the extremes in terms of LACs, 0 cm^{-1} for air and 0.150 cm^{-1} and higher for cortical bone (10).

The pros and cons of the segmentation-based MR-AC methods are summarized in Table 1.

First steps—The first MR segmentation method was reported in 1994. It focused on the brain and used a surface registration algorithm to align the MR (a T1-weighted image) with the PET image (11). Once in the same space, the MR images were segmented using morphological operations combined with hard thresholds to obtain brain, skull and skin. LACs were finally assigned to each tissue class: 0.095 cm^{-1} to brain and skin and 0.151 cm^{-1} to bone. Almost a decade later, an improved approach was proposed in which the coregistered MR (also a T1-weighted image) was segmented, via a fuzzy clustering algorithm, into 4 classes: air, skull, brain tissue and nasal sinuses (12).

State of the Art—Since 2009, a number of proposed methods generated promising results. We could group these methods into two main classes: *UTE-based approaches*, that use an ultra-short echo time (UTE) MR sequence to provide signal from bone tissues; and *non UTE-based approaches* that rely on other types of MR sequences.

UTE-based: In 2010, both Keereman et al. and Catana el al. independently used for the first time a UTE sequence to obtain signal from bone tissue, which helped with its segmentation from the rest of the tissue classes (13, 14). Catana et al. used the difference of the two echoes divided by the second echo squared to enhance bone voxels and the sum of the two echoes divided by the first echo squared to enhance voxels corresponding to air (Fig. 4) (14). Keereman et al. used the inverse of the spin-spin relaxation time T2, called relaxation rate or

simply R2, to segment bone from the other tissue classes. The R2 was defined as the difference of the logarithmic echo images over the difference of the echo times (13). In a modified version of this approach, the magnetic field was dynamically monitored by using a magnetic field camera, which allowed the correction of the k-space trajectory distortions induced by the eddy currents artifacts (15). A new Dixon-based strategy to obtain relaxation rates (R2*) from UTE sequences was used in (16). Interestingly, the authors also explored and optimized the k-space sampling to reduce the acquisition time by 75%, while preserving the image quality and contrast in cortical bone.

Two different methods to convert the relaxation times R2* into continuous CT values have recently been explored. The first used a regression analysis to map the R2* values into pseudo-CT values via a 5-parameter sigmoid function (17). In the second approach, the R2* data was equalized with either patient-specific CT data (if available) or with generic population CT data to obtain continuous pseudo-CT values (18).

Combinations of sequences have also been explored in this context. A new triple-echo sequence (called UTILE) that combined UTE and the Dixon techniques was developed to segment air, fat, soft tissue and bone for brain imaging (19). In (20) fuzzy C-means were used to segment the data acquired with T1-weighted, T2-weighted, UTE, time-of-flight (ToF) and Dixon sequences to segment skull, fat, soft tissue and air.

Recently, a sequence that allows the acquisition of the echo signal (known as free induction decay, or FID) immediately after the end of the excitation was proposed for bone imaging. This sequence is known as zero echo time, or ZT sequence. A ZT-type sequence, called RUFIS (rotating ultra-fast imaging sequence), has been shown to capture more efficiently the short T2* signal from bone tissues while additionally having a flat proton-density (PD) response in soft tissues (21). A clinical evaluation of the use of ZT sequence has also been recently performed in 15 subjects (22) showing great potential to produce CT-like images (Fig. 5).

Non UTE-based: As mentioned previously, currently the only three whole-body FDA-approved AC methods for PET/MRI belong to this category. Interestingly, none of them provides bone as a separate tissue class but are applied to brain and **whole-body** imaging, except in the case of the GE approach that uses an atlas for brain images. The first one uses a Vibe Dixon sequence with in- and out-of-phase images to separate fat- from water-based tissues (8). This Dixon-based method produces an attenuation map with 4 tissue classes: air, soft-tissue, fat and lungs, with the lungs obtained as the connected air class inside the body. The AC approach initially implemented on the Siemens Biograph mMR scanner was based on this method (2). A similar approach is followed for whole-body on the GE Signa PET/MR scanner using the Dixon sequence to provide continuous fat/water AC values, lung and air (9). The third one, implemented on the Philips Ingenuity TF scanner, classified a T1-weighted image into 3 tissues: soft-tissue, air or lungs (6, 7). A similar 3-class segmentation approach was also tested on beagles using T1-weighted images and compared with a 4-class approach including bone from a registered CT (23).

The use of fuzzy classifiers has recurrently been proposed for segmentation. A minimal path segmentation approach (similar to segmentation with snakes) was implemented followed by a multiscale fuzzy C-mean classifier for brain images (24). This approach was subsequently improved by including a Radon transform of the MR image (T1-weighted) to segment the skull from the brain (25, 26).

"Take home" comparative results—Fig. 6 shows a comparative plot of the MR-AC segmentation-based methods. Only data available in the original manuscripts are included. Despite our efforts to include comparable values in this plot, as well as in Fig. 9 and Fig. 12, care must be taken when comparing them since the methodology followed varied from study to study.

Atlas-based methods

Rationale—Atlas-based methods use a dataset (or multiple datasets) for which the LACs are known or could be derived from (e.g. CT images). The dataset is then mapped into the subject specific MR space, either via non-rigid coregistration (using the atlas as a template) or via probabilistic methods. Although not necessarily, in most cases the atlases are composed of pairs of image datasets: the atlas MR image (generated from data acquired with a similar MR sequence to the one to be used for the new subjects) and the atlas image with the LACs information (i.e. transmission or CT images).

Challenges, Pros and Cons—The major challenge for atlas-based methods is the difficulty in warping local anatomical variants, particularly for the whole-body case. However, atlas-based methods provide bone information and continuous attenuation values that tend to improve the final PET image quantification when compared to segmented approaches. A summary of the pros and cons of the atlas-based MR-AC approaches is shown in Table 2.

First steps—The first atlas-based method used the well-known SPM2 (Statistical Parametric Mapping, UCL) to spatially normalize the PET image of the subject to the PET image of an atlas and the corresponding atlas transmission image (27). The transmission image was then warped back into the (PET) subject space using the inverse deformations estimated during the spatial normalization process. As a result, a subject-specific transmission image is generated in subject (PET) space. A similar strategy using SPM2 was used to spatially normalize the subject images to an atlas composed of transmission images and T1-weighted MR images (instead of the PET images as in the previous case) (28). Both studies showed comparable results, the mean differences in the brain being ~10%.

State of the Art—Atlas-based methods could be further classified into two main groups: the *template-based* approaches, where the template images are non-rigidly warped back into the subject space (like in the first methods); and *probabilistic-based* approaches, where the atlas information is used via probabilistic or machine learning techniques to generate a pseudo-CT image. Additionally, a third group could be defined, the *mixed-based* approaches that includes those methods combining elements from the first two approaches.

Template-based: In this group we find the first method specifically implemented for **whole-body** applications (besides the two segmentation-based methods presented above). The approach used a non-rigid algorithm to register the atlas CT images to the subject MR image and a histogram-matching algorithm to map MR values into final pseudo-CT values (29). The method was tested for head and neck, thoracic, abdominal and pelvic imaging with errors larger than 10% in some regions.

A non-rigid algorithm based on optical flow was used to coregister the template CT to the subject MR image in (30). While the authors showed excellent agreement between the CT and pseudo-CT images obtained (with a mean difference in all voxels of 2 HU), only data from a single PET study was shown and no figures of merit (such as relative differences or similar) were given. Malone et al. compared the SPM2 and B-splines non-rigid algorithms for coregistration of the atlas MR images into the subject MR, using either a tissue phantom or a transmission template as atlas pairs together with the MRs (Fig. 7) (31). The authors concluded based on the analysis of reconstructed PET brain images that the transmission template approach was better than the tissue phantom, and that B-splines was better than SPM2 (31). In a different approach, an atlas was composed of 121 CT scans and weighted heuristic measures were used to choose the “most similar” CT to the subject’s MR in terms of body geometry, which was non-rigidly coregistered to the subject’s MR (32). Two segmentation-based methods were generated and compared: the standard 4-tissue segmentation (air, fat, soft tissue and lung) and a second one that included additionally the bone derived from the warped atlas CT image. The comparisons showed that the method including the atlas-CT bone reduced the errors in bone and adjacent regions of interest (ROIs), however the “correlation coefficient was essentially unchanged in all tissues regardless of whether bone was included or not” (32).

A brain atlas-based approach combining non-rigid coregistration plus similarity measurements was used to generate a pseudo-CT image (33, 34). The technique non-rigidly registers the atlas MR images into the subject MR image (all MRs are T1-weighted images) and uses the resulting deformations to warp the atlas CTs into subject space. Instead of using an average of all the warped CTs the approach calculates similarities between each warped MR atlas image and the original subject image by using a convolution-based fast local normalized correlation coefficient similarity measure. The final pseudo-CT image is generated by a linear combination of all atlas-CT images weighted by an exponential function of the ranked similarities (33). The method was optimized using 18 subjects and then it was successfully tested on another 41 subjects using the subject PET reconstructed with CT-AC as the gold-standard and comparing the results with a UTE-based segmentation method (air, soft tissue and bone) as well as to the best warped CT image from the atlas (34). As a way to obtain warped CT images closer to the subject space, an iterative scheme was chosen to re-coregister the warped atlas CTs to their mean until convergence. Finally, a median filter was applied to obtain the final pseudo-CT from all the warped CTs (35).

Probabilistic-based: The use of probabilistic and machine learning techniques has grown in the recent years due to their potential to benefit whole-body applications and the quality of their results. A Gaussian Mixture Regression (GMR) approach was used to generate pseudo-CT images from the subject MR images (36). The atlas images consisted of 1 CT image and

15 MR images per subject, consisting of 3 versions (original, mean and standard deviation images) of the images acquired with each of the following 5 MR sequences: the two echoes of two different UTE acquisitions (with different flip angles) and one T2-weighted. For any new subject the same 5 MR images (generating the 15 MR datasets) were acquired and the regression model was applied to then generate a pseudo-CT image (36). In later studies the authors found that the T2-weighted sequence was redundant in terms of the information provided and therefore was dropped from the regression model (37). A comparative study of the resulting PET images showed results comparable to those obtained using the real CTs (38). Additional improvements have been demonstrated by adding spatial information (39) as well by reducing the acquisition time for the UTE sequences with parallel imaging (40). A similar approach but using support vector regression (SVR) machinery instead of GMR was used to model the mapping between the atlas CT and MR images (using a UTE and a Dixon sequence, with image features extracted for mean, median, variance, maximum and minimum) (41). Once trained, the SVR machinery was applied to predict a pseudo-CT image from the subject MR images. Although the authors mostly focused on the brain with great results, the method was also used to generate the attenuation map of the pelvis for one subject, which suggest it could be used for **whole-body** imaging as well (41).

Despite their high computational cost, *patch-based* methods have recently received renewed attention due to their robustness and potential adaptability to whole-body applications. They use local probabilistic and similarity measures to compare a region (known as *patch*) of the subject's MR image to the whole MR database. The best patch (or patches) from the atlas database that fits the subject is chosen and its corresponding CT patch is used to obtain a pseudo-CT image. The first implementation of a patch-based approach combined it with a non-rigid registration to an atlas and a classic segmentation-based method (42). The method was initially tested for brain imaging but subsequently applied to **whole-body** imaging, showing results superior to the segmentation-based method with 5 classes (lung, bone, fat, soft tissue and a mixture of fat and soft tissue) (43). Others have also proposed pure patch-based approaches for brain imaging, either using T1-weighted images combined with probabilistic air maps to separate bone and air (44) or the two UTE echoes as atlases in addition to a Gaussian mixture model (GMM) to provide all convex linear combinations of pairs of atlases to reduce the sparsity problem linked to patch-based methods (45). To address the large computational cost, a GPU-based algorithm based on a weighted linear combination of the atlas CT images with weights based on their similarity was proposed (46).

Mixed-based: An atlas-guided segmentation technique has demonstrated improved results when compared to the original UTE-based only approach for brain imaging (47). More recently, it has been shown that a combination of segmentation- and atlas-based features confers flexibility to adapt to the local anatomical variants of the subject (thanks to the segmentation step), and robustness thanks to the non-rigid diffeomorphic registration to a template (48). This approach, developed using the SPM8 software for both the image segmentation and non-rigid coregistration steps, generated very good results using datasets acquired at different institutions (48). Similarly, Anazodo et al. used an SPM8-based

approach to combine the Dixon-based method with the bone segmentation generated from SPM8 (49).

"Take home" comparative results—Fig. 9 shows a comparative plot of the MR-AC atlas-based methods.

PET-AC

Rationale—PET-AC methods aim at using the emission PET data that inherently contain information about the attenuation, o derive the LACs. Therefore these methods are well suited for whole-body applications, although in most cases they require a non-specific radiotracer to provide information for all tissues. There are three main classes of PET-AC methods: approaches that derive attenuation maps by post-processing the emission images (*emission-based*); approaches that aim to jointly estimate emission and attenuation (*joint estimation-based* methods) using iterative algorithms based on maximum likelihood (ML); and approaches that use external transmission sources to derive the LACs (*Tx-based*). Since no MR images are required (in principle) for the PET-AC methods, approaches in this category were developed earlier compared to the other MR-AC methods, to be used in standalone PET (and PET/CT) scanners.

Challenges, Pros and Cons—Until recently, post-processing the emission data allowed only the approximate estimation of the actual LACs (segmented AC maps). Deriving emission and attenuation images jointly from the PET raw data is a "very ill-posed problem" that results in crosstalk between both estimations (50–52). Cross-talk is characterized by the presence of localized errors in the emission map which are compensated by errors in the attenuation map. Solving the cross-talk problem requires additional information, either *a priori* (from MR or other imaging modality) or ToF information. Joint estimation requires also that sufficient counts are recorded in all the lines of response that intersect the attenuation map. Finally, the Tx-based approaches, considered the real "gold-standard" for AC in PET as they measure the attenuation at PET energy levels (and are more immune to metal artifacts), involve additional radiation exposure to the subject (although minimal compared to PET or CT scans), an extended acquisition time (unless the transmission and emission data are collected simultaneously), an increase in detector dead-time and tend to produce more noisy estimations of the LACs. A summary of the pros and cons of the PET-AC approaches is shown in Table 3.

First steps—Because PET-AC methods were developed for standalone PET scanners, the first Tx-based approach was reported in 1975 and used a ring of ^{64}Cu positioned around the subject (a dog in this case) (53). The first joint-based algorithm was also developed before the first PET/MR was introduced and used a ML estimator with an EM (Expectation-Maximization) scheme (50). The method applied kernel sieves to constrain the solution and minimize its bias.

State of the Art

Emission-based: Prior to PET/MR scanners, emission-based approaches were developed to either reduce the noise and variability of the transmission images or completely replace the

transmission scans to reduce both the radiation exposure and acquisition times. In an early method, simple segmented attenuation maps were obtained from the emission data using the sinogram information (54). The same information was also used to segment and estimate the LACs for the skull and the rest of the brain (5). More recently a 3-step PET reconstruction process was used to segment lungs and body contour from the intermediate PET reconstructed images (55).

Finally, the scatter information has been proposed to derive LACs using a two-level approach: a scatter-to-attenuation reconstructor and a scatter-to-attenuation back projector (56). Although the method is still in its initial development phase and comes with an extremely large computational cost, very interesting and promising results have been demonstrated with simulated data.

Joint estimation-based: The joint estimation of transmission and emission images was first demonstrated using an ML algorithm (57). In a similar approach, the simultaneous estimation was performed after the two images were initially estimated separately (58). Nuyts et al. extended the use of simultaneous joint estimation without the need of transmission images, in an approach called ML reconstruction of attenuation and activity (MLAA) (51). ToF information was incorporated subsequently in (59) and (60) to reduce the cross-talk, although this was shown to determine the attenuation map sinogram (for all lines of response where activity is present) only up to a constant factor (61). This constant factor can be determined by imposing an *a priori* knowledge of the attenuation value in a portion of the attenuation map. A recently developed method using GMM in addition to ToF information (62) was shown to be superior to the standard 4-class MR-AC (Fig. 10) as well as to the standard MLAA methods discussed above (63).

Tx-based: Finally, the use of transmission sources seems to be having its second youth with PET/MRI. The use of an annulus transmission source combined with the ToF information was demonstrated in (64) and two years later was applied to real PET studies in humans (65). A single ring transmission source and a multi-bed transmission-emission strategy was recently proposed for non-ToF capable PET/MR scanners (66). An interesting alternative uses the background radiation of the LSO scintillators to simultaneously acquire emission and transmission images using different energy windows and the ToF information (67).

“Take home” comparative results—Fig. 12 shows a comparative plot of the PET-AC methods.

MR-AC: sources of artifacts and other challenges

In addition to accurately translate the MR information into precise LACs, the MR-AC methods need to minimize the potential impact of artifacts in the PET/MR images that could bias the estimation of the LACs. For example, artifacts caused by metallic implants within the MR FoV or truncation due to limited MR FoV need to be considered. Additionally, the attenuation of hardware components present in the FoV of the PET/MR scanner, such as MR RF coils and other equipment (headphones, positioning aids, etc.) has to be accounted for.

A very challenging region for whole-body AC is the thorax because the lung tissue exhibits large intra- and inter-subject density variability (68, 69) and only a handful of studies have tackled this problem. A method to relate the MRI and CT signals from the lungs was developed in (70). Pulmonary lesions were evaluated with the Dixon-method in (71) and the use of PET/MR in lung cancer was examined in (72). Additionally, motion impacts the accuracy of AC methods and is even more critical in whole-body imaging due to the combination of physiological and non-physiological subject motion. Motion correction in PET/MR is a separate very active area of research and we refer the interested reader to a dedicated review focused on challenges and potential solutions (73). This section will review the latest approaches to address these issues. We have grouped them into three main categories: *body-truncation correction*, *foreign object correction* (such as metallic implants) and *hardware correction* (such as MR flexible coils).

Body-truncation correction

Body-truncation artifacts occur due to the limited effective FoV of the MRI compared to that of the PET scanner. In the case of relatively large subjects, the MR images may not include the whole subject's anatomy, which impacts the performance of the MR-AC approaches. It has been shown that the bias introduced by incomplete attenuation maps is on average 15% but could locally reach up to 50% (74). A truncation-correction method was proposed for segmenting the body contour with a 3D snake algorithm from the PET images reconstructed with incomplete attenuation information. Even with this method, local errors of up to 20% were still obtained near the edge of the MR FoV. A similar method used the PET data reconstructed with incomplete attenuation information to obtain the body contour of the subject and was compared to the manufacturer's algorithm that obtained the body contour from the PET non-attenuation corrected (NAC) image (75). A maximum-a-posteriori (MAP) algorithm was included as a modification of the original MLAA approach for estimating the truncated areas of the body in the attenuation map (76). The method was tested in simulated data and in one PET/MR subject.

Finally, a new method to extend the MR FoV was based on a technique called homogenization using gradient enhancement (HUGE) in which gradient fields are used to correct for field inhomogeneities and nonlinearities (77). This method was later used to minimize the body truncation in 12 PET/MR subjects (78) and showed improvements in PET image quantification compared to the Dixon-method as well to the previously mentioned MAP MLAA-based method.

Foreign object correction

Metallic implants tend to produce a large signal void in the MR images (79) (and streaking artifacts in CT images (80)), which bias the PET image quantification when MR-AC methods are used.

Three alternatives to the original Dixon-method were suggested to correct for the effect of MR artifacts due to metallic implants in the pelvic area. The first was to fill the signal void with soft tissue. In the second case, a coregistered CT attenuation map of the implant was superimposed on the map generated above. In the third case, the signal void was filled with

metal (81). Not surprisingly, the conclusion was that the second approach was the best. A modified version of the patch-based method shown in (43) added an extra class to include low MR signal regions (due to either air pockets inside the gastrointestinal tract or metallic implants) (82). Separation of air pockets and metallic implant areas was then performed via an atlas that provided *a priori* information of probable metallic implant areas.

Newer MR sequences can also be used to minimize the extent of the artifacts. A multiacquisition variable resonance image combination (MAVRIC) MR sequence was used to reduce metal artifacts from dental implants and improve the performance of the MR-AC when compared to the conventional Dixon-method (83). The MAVRIC sequence requires long acquisition times and therefore its use is only justified in very specific areas where the implants are located.

The impact of MR contrast agents on PET image quantification was also studied by Lois et al. (84). They concluded that these agents are not expected to significantly impact the PET image quantification but oral iron-oxide contrasts might bias the MR-AC maps.

It is worth mentioning in this context that the effects of image artifacts as well as other data inconsistencies (in the attenuation map for instance) are supposed to be reduced in ToF capable scanners (85). Recent studies have confirmed these theoretical predictions as shown in (86–88).

Hardware correction

MR coils and other devices are generally “invisible” to the MRI scanner. However, they are not invisible to the PET photons and generally induce extra attenuation that if not properly accounted for could potentially lead to large image bias and artifacts. The importance of accounting for the attenuation properties of the MR hardware has been demonstrated using high-exposure CT images (89). The study also showed that accurate coregistration (below 1–2 mm) is mandatory to avoid important attenuation-driven artifacts. Similar studies showing the impact of surface coils have also been performed (90–92). Paulus et al. developed for the first time a method to correct for MR surface coils (93). They used MR visible markers (cod liver oil capsules) positioned on top of the coils to allow for accurate non-rigid registration of the coil to its CT-derived template (93). The same authors also provided an improved conversion of the CT image of the coil template to LACs at PET energy levels (511 keV) (94). A similar non-rigid coregistration of the flexible coils to its attenuation template has been suggested in (95).

Finally, certain positioning aids, such as vacuum mattresses, were also shown to bias the PET images (96). Similarly, the use of headphones in PET/MR studies could result in an underestimation in local areas from 1.9% to 13.2% (97).

Current Status of MR-AC for Clinical PET/MRI Studies

Since the introduction of the first human combined PET/MR scanner in 2008 and the first whole-body PET/MR in 2010, there has been a lot of interest in addressing the challenges and demonstrating the benefits of this technology. Recognizing the qualitative and

quantitative effects of MR-AC on the PET images has led to the myriad of methods that were reviewed here. Additionally, a large number of studies have compared the different methods to better understand their benefits and/or limitations. Finally, more and more clinical evaluation and comparison studies have also been carried out.

Clinical Studies Evaluating MR-AC methods

The need to account for bone in MR-AC methods has been demonstrated in several studies (98–101). The 3-class segmentation MR-AC method implemented on the Philips sequential PET/MR scanner was compared to the transmission-based AC in (102) and to the CT-AC in (103) and (69). This latter study compared the MR-AC methods in two groups, with and without the MR coils in the FoV, as well as performing a clinical evaluation and comparison of all PET reconstructed images, including the frequency and effects of artifacts in the attenuation map and the PET reconstructed images (69). The authors concluded that the presence of the coils in the FoV increases the variability in PET image quantification and that MR-AC compared to CT-AC introduces a bias of around 10% in whole-body, with some ROIs showing larger differences (e.g. spine, lung and heart). The same comparison to CT-AC was also performed in a pre-clinical model and showed comparable results (104).

Andersen et al. compared the Dixon-method (4-class segmentation) implemented on the Siemens PET/MR scanner to the CT-AC method for brain imaging, demonstrating once again the need to include bone to avoid large radial biases across the brain (105). A whole-body comparison of the Dixon-based to the CT-AC method was also performed in (106) showing large bias in individual subjects (of up to 22%), which according to the authors “is significant during clinical follow-up exams”. A study of the impact of artifacts on the Dixon-based method was performed retrospectively on 100 PET/MR patients with 276 artifacts (107). The study showed that 21% of the avid-PET lesions detected were affected by artifacts, mostly without clinical consequences except in 9 lesions that could have been missed because of the artifacts. The authors clarified that the combined use of the PET-NAC or additional MR images helped with the detection of these lesions so the clinical diagnosis would not be affected by the biased maps (107).

A comparison of the Dixon- and UTE-based methods (also implemented on the Siemens PET/MR scanner, (13)) versus CT-AC was done for brain imaging in (108). The authors showed large underestimations with both methods Dixon- and UTE-based when compared to CT-AC. Delso et al. also compared the same UTE-based method versus CT-AC for brain imaging and concluded that in some areas the UTE-method led to bias and that more sophisticated methods may be needed (109).

Finally, the performance of the Philips 3-class segmentation and the Siemens 4-class segmentation method were compared to the CT-AC. Large biases were observed for both MR-AC methods and the authors suggested the need of checking the attenuation map for potential artifacts that could bias the SUV measurements (110).

Clinical Studies Highlighting the Importance of Accurate AC

Clinical evaluation of the impact of artifacts in the MR-AC has been performed in several studies, such as the previously mentioned (69) and (110), but also in (111), where similar

conclusions were drawn: the use of PET-AC together with PET-NAC and other MR images improves the detection of artifact-driven bias in the images and “ensure clinically accurate image interpretation”.

The Dixon-method has been clinically evaluated in multiple occasions. In the early studies it was shown to be valid for “anatomical allocation of PET-positive lesions, similar to low-dose CT in conventional PET/CT” (112) as well as for oncologic studies (113). Fraum et al. discussed MR-AC in the context of abdominal and pelvic oncological PET/MR use (114) while Schafer et al. compared MR-AC and CT-AC in pediatric oncological subjects (115). The authors concluded that SUV quantification was similar and the rates of lesion detection were equivalent, with the advantage of the lower radiation exposure from the PET/MR (115). The Dixon-method in PET/MR was also compared to contrast-enhanced CT in PET/CT for whole-body in 12 subjects with different malignant disorders (116). The study concluded that despite the differences in AC both methods correlated well in PET-positive lesions. However the use of the Dixon sequence alone was not deemed to provide adequate anatomic information due to its low resolution and the use of other MR sequences was encouraged (116). In (117) the Dixon-based method was compared to CT-AC in 30 subjects with suspected dementia. Differences were observed in the PET/MR images compared to the PET/CT but such differences “may only in part be explained by inconsistencies in the attenuation-correction procedures” (117).

The 3-class segmentation implemented on the Philips system was also clinically evaluated for head-and-neck cancers in 32 subjects with equivalent performance to PET/CT as reported in (118). In lymph node cancer it also showed “a strong parallel to PET/CT in terms of SUVmax, interobserver agreement and diagnostic performance” (119).

Finally, the use of PET/MRI with the UTE-based method was compared to PET/CT in 16 subjects with various neurological indications. The study concluded that the “PET quantitation accuracy using the MRI based UTE sequences for AC in simultaneous brain PET/MRI is reliable in a clinical setting, being similar to that obtained using PET/CT” (71).

Conclusions and Future of AC for PET/MRI

There has been an explosion of methods developed to overcome the challenging task of AC in PET/MRI scanners. Comparative studies very strongly suggest that bone attenuation needs to be accounted for not only for accurate quantification but also to avoid potential clinical misinterpretation. It appears that combined methods might provide more accurate and robust results as the synergistic combination of their strengths can be used to overcome their individual limitations.

Regarding artifacts (implants, truncation, etc.) it is quite clear that more robust methods are required to reduce their effect on the final PET images. New MR sequences, such as ZT, MAVRIC, HUGE and others could potentially offer innovative solutions to overcome such problems and improve the MR-AC solutions.

Moving forward, MR-AC methods will need to be developed for more robust estimation of whole-body attenuation maps, particularly in the lungs.

References

1. Keereman V, Mollet P, Berker Y, Schulz V, Vandenberghe S. Challenges and current methods for attenuation correction in PET/MR. MAGMA. 2013; 26:81–98. [PubMed: 22875599]
2. Bezrukov I, Mantlik F, Schmidt H, Scholkopf B, Pichler BJ. MR-Based PET Attenuation Correction for PET/MR Imaging. Semin Nucl Med. 2013; 43:45–59. [PubMed: 23178088]
3. Huang SC, Hoffman EJ, Phelps ME, Kuhl DE. Quantitation in positron emission computed tomography: 2. Effects of inaccurate attenuation correction. J Comput Assist Tomogr. 1979; 3:804–814. [PubMed: 315970]
4. Bergstrom M, Litton J, Eriksson L, Bohm C, Blomqvist G. Determination of object contour from projections for attenuation correction in cranial positron emission tomography. J Comput Assist Tomogr. 1982; 6:365–372. [PubMed: 6978896]
5. Weinzapfel BT, Hutchins GD. Automated PET attenuation correction model for functional brain imaging. J Nucl Med. 2001; 42:483–491. [PubMed: 11337527]
6. Hu, Z., Ojha, N., Renisch, S., et al. MR-based attenuation correction for a whole-body sequential PET/MR system. Paper presented at: Nuclear Science Symposium Conference Record (NSS/MIC), 2009 IEEE; 2009;
7. Schulz V, Torres-Espallardo I, Renisch S, et al. Automatic, three-segment, MR-based attenuation correction for whole-body PET/MR data. Eur J Nucl Med Mol Imaging. 2011; 38:138–152. [PubMed: 20922522]
8. Martinez-Moller A, Souvatzoglou M, Delso G, et al. Tissue classification as a potential approach for attenuation correction in whole-body PET/MRI: evaluation with PET/CT data. J Nucl Med. 2009; 50:520–526. [PubMed: 19289430]
9. Wollenweber SD, Ambwani S, Lonn AH, et al. Comparison of 4-Class anc Continuous Fat/Water Methods for Whole-Body, MR-Based PET Attenuation Correction. IEEE Trans Nucl Sci. 2013; 60:3391–3398.
10. Kinahan PE, Townsend DW, Beyer T, Sashin D. Attenuation correction for a combined 3D PET/CT scanner. Med Phys. 1998; 25:2046–2053. [PubMed: 9800714]
11. Le Goff-Rougetet R, Frouin V, Mangin J-F, Bendriem B. Segmented MR images for brain attenuation correction in PET. Proc SPIE. 1994; 2167:725–736.
12. Zaidi H, Montandon ML, Slosman DO. Magnetic resonance imaging-guided attenuation and scatter corrections in three-dimensional brain positron emission tomography. Med Phys. 2003; 30:937–948. [PubMed: 12773003]
13. Keereman V, Fierens Y, Broux T, De Deene Y, Lonneux M, Vandenberghe S. MRI-based attenuation correction for PET/MRI using ultrashort echo time sequences. J Nucl Med. 2010; 51:812–818. [PubMed: 20439508]
14. Catana C, van der Kouwe A, Benner T, et al. Toward implementing an MRI-based PET attenuation-correction method for neurologic studies on the MR-PET brain prototype. J Nucl Med. 2010; 51:1431–1438. [PubMed: 20810759]
15. Aitken AP, Giese D, Tsoumpas C, et al. Improved UTE-based attenuation correction for cranial PET-MR using dynamic magnetic field monitoring. Med Phys. 2014; 41:012302. [PubMed: 24387523]
16. Hu L, Su KH, Pereira GC, et al. k-space sampling optimization for ultrashort TE imaging of cortical bone: applications in radiation therapy planning and MR-based PET attenuation correction. Med Phys. 2014; 41:102301. [PubMed: 25281971]
17. Juttukonda MR, Mersereau BG, Chen Y, et al. MR-based attenuation correction for PET/MRI neurological studies with continuous-valued attenuation coefficients for bone through a conversion from R2* to CT-Hounsfield units. Neuroimage. 2015; 112:160–168. [PubMed: 25776213]
18. Cabello J, Lukas M, Forster S, Pyka T, Nekolla SG, Ziegler SI. MR-Based Attenuation Correction Using Ultrashort-Echo-Time Pulse Sequences in Dementia Patients. J Nucl Med. 2015; 56:423–429. [PubMed: 25678486]
19. Berker Y, Franke J, Salomon A, et al. MRI-based attenuation correction for hybrid PET/MRI systems: a 4-class tissue segmentation technique using a combined ultrashort-echo-time/Dixon MRI sequence. J Nucl Med. 2012; 53:796–804. [PubMed: 22505568]

20. Hsu SH, Cao Y, Huang K, Feng M, Balter JM. Investigation of a method for generating synthetic CT models from MRI scans of the head and neck for radiation therapy. Phys Med Biol. 2013; 58:8419–8435. [PubMed: 24217183]
21. Wiesinger F, Sacolick LI, Menini A, et al. Zero TE MR bone imaging in the head. Magn Reson Med. 2015
22. Delso G, Wiesinger F, Sacolick LI, et al. Clinical Evaluation of Zero-Echo-Time MR Imaging for the Segmentation of the Skull. J Nucl Med. 2015; 56:417–422. [PubMed: 25678489]
23. Steinberg J, Jia G, Sammet S, Zhang J, Hall N, Knopp MV. Three-region MRI-based whole-body attenuation correction for automated PET reconstruction. Nucl Med Biol. 2010; 37:227–235. [PubMed: 20152722]
24. Fei B, Yang X, Wang H. An MRI-based Attenuation Correction Method for Combined PET/MRI Applications. Proc SPIE Int Soc Opt Eng. 2009:7262.
25. Fei B, Yang X, Nye JA, et al. MRPET quantification tools: registration, segmentation, classification, and MR-based attenuation correction. Med Phys. 2012; 39:6443–6454. [PubMed: 23039679]
26. Yang X, Fei B. Multiscale segmentation of the skull in MR images for MRI-based attenuation correction of combined MR/PET. J Am Med Inform Assoc. 2013; 20:1037–1045. [PubMed: 23761683]
27. Montandon ML, Zaidi H. Atlas-guided non-uniform attenuation correction in cerebral 3D PET imaging. Neuroimage. 2005; 25:278–286. [PubMed: 15734362]
28. Kops ER, Herzog H. Alternative methods for attenuation correction for PET images in MR-PET scanners. Nuclear Science Symposium Conference Record. 2007; 6:4327–4330.
29. Beyer T, Weigert M, Quick HH, et al. MR-based attenuation correction for torso-PET/MR imaging: pitfalls in mapping MR to CT data. Eur J Nucl Med Mol Imaging. 2008; 35:1142–1146. [PubMed: 18283452]
30. Schreibmann E, Nye JA, Schuster DM, Martin DR, Votaw J, Fox T. MR-based attenuation correction for hybrid PET-MR brain imaging systems using deformable image registration. Med Phys. 2010; 37:2101–2109. [PubMed: 20527543]
31. Malone IB, Ansorge RE, Williams GB, Nestor PJ, Carpenter TA, Fryer TD. Attenuation correction methods suitable for brain imaging with a PET/MRI scanner: a comparison of tissue atlas and template attenuation map approaches. J Nucl Med. 2011; 52:1142–1149. [PubMed: 21724984]
32. Marshall HR, Patrick J, Laidley D, et al. Description and assessment of a registration-based approach to include bones for attenuation correction of whole-body PET/MRI. Med Phys. 2013; 40:082509. [PubMed: 23927354]
33. Burgos N, Cardoso MJ, Modat M, et al. Attenuation correction synthesis for hybrid PET-MR scanners. Med Image Comput Comput Assist Interv. 2013; 16:147–154.
34. Burgos N, Cardoso MJ, Thielemans K, et al. Attenuation correction synthesis for hybrid PET-MR scanners: application to brain studies. IEEE Trans Med Imaging. 2014; 33:2332–2341. [PubMed: 25055381]
35. Sjolund J, Forsberg D, Andersson M, Knutsson H. Generating patient specific pseudo-CT of the head from MR using atlas-based regression. Phys Med Biol. 2015; 60:825–839. [PubMed: 25565133]
36. Johansson A, Karlsson M, Nyholm T. CT substitute derived from MRI sequences with ultrashort echo time. Med Phys. 2011; 38:2708–2714. [PubMed: 21776807]
37. Johansson A, Karlsson M, Yu J, Asklund T, Nyholm T. Voxel-wise uncertainty in CT substitute derived from MRI. Med Phys. 2012; 39:3283–3290. [PubMed: 22755711]
38. Larsson A, Johansson A, Axelsson J, et al. Evaluation of an attenuation correction method for PET/MR imaging of the head based on substitute CT images. MAGMA. 2013; 26:127–136. [PubMed: 22955943]
39. Johansson A, Garpebring A, Karlsson M, Asklund T, Nyholm T. Improved quality of computed tomography substitute derived from magnetic resonance (MR) data by incorporation of spatial information--potential application for MR-only radiotherapy and attenuation correction in positron emission tomography. Acta oncologica. 2013; 52:1369–1373. [PubMed: 23984810]

40. Johansson A, Garpebring A, Asklund T, Nyholm T. CT substitutes derived from MR images reconstructed with parallel imaging. Med Phys. 2014; 41:082302. [PubMed: 25086551]
41. Navalpakkam BK, Braun H, Kuwert T, Quick HH. Magnetic resonance-based attenuation correction for PET/MR hybrid imaging using continuous valued attenuation maps. Invest Radiol. 2013; 48:323–332. [PubMed: 23442772]
42. Hofmann M, Steinke F, Scheel V, et al. MRI-based attenuation correction for PET/MRI: a novel approach combining pattern recognition and atlas registration. J Nucl Med. 2008; 49:1875–1883. [PubMed: 18927326]
43. Hofmann M, Bezrukov I, Mantlik F, et al. MRI-based attenuation correction for whole-body PET/MRI: quantitative evaluation of segmentation- and atlas-based methods. J Nucl Med. 2011; 52:1392–1399. [PubMed: 21828115]
44. Chen Y, Juttukonda M, Su Y, et al. Probabilistic Air Segmentation and Sparse Regression Estimated Pseudo CT for PET/MR Attenuation Correction. Radiology. 2014:140810.
45. Roy S, Wang WT, Carass A, Prince JL, Butman JA, Pham DL. PET attenuation correction using synthetic CT from ultrashort echo-time MR imaging. J Nucl Med. 2014; 55:2071–2077. [PubMed: 25413135]
46. Torrado-Carvajal A, Alcain E, Herraiz JL, et al. A Fast Patch-Based Approach for Pseudo-CT Generation from MRI T1-Weighted Images: A Potential Solution for PET/MR Attenuation Correction. ISMRM. 2015
47. Poynton CB, Chen KT, Chonde DB, et al. Probabilistic atlas-based segmentation of combined T1-weighted and DUTE MRI for calculation of head attenuation maps in integrated PET/MRI scanners. American journal of nuclear medicine and molecular imaging. 2014; 4:160–171. [PubMed: 24753982]
48. Izquierdo-Garcia D, Hansen AE, Forster S, et al. An SPM8-based approach for attenuation correction combining segmentation and nonrigid template formation: application to simultaneous PET/MR brain imaging. J Nucl Med. 2014; 55:1825–1830. [PubMed: 25278515]
49. Anazodo UC, Thiessen JD, Ssali T, et al. Feasibility of simultaneous whole-brain imaging on an integrated PET-MRI system using an enhanced 2-point Dixon attenuation correction method. Front Neurosci. 2014; 8:434. [PubMed: 25601825]
50. Clinthorne, NH., Fessler, JA., Hutchins, GD., Leslie Rogers, W. Joint Maximum Likelihood Estimation of Emission and Attenuation Densities in PET. Paper presented at: IEEE Trans. Nucl. Sci. Symp. Med. Im. Conf; 1991;
51. Nuyts J, Dupont P, Stroobants S, Benninck R, Mortelmans L, Suetens P. Simultaneous maximum a posteriori reconstruction of attenuation and activity distributions from emission sinograms. IEEE Trans Med Imaging. 1999; 18:393–403. [PubMed: 10416801]
52. Landmann M, Reske SN, Glatting G. Simultaneous iterative reconstruction of emission and attenuation images in positron emission tomography from emission data only. Med Phys. 2002; 29:1962–1967. [PubMed: 12349915]
53. Phelps ME, Hoffman EJ, Mullani NA, Ter-Pogossian MM. Application of annihilation coincidence detection to transaxial reconstruction tomography. J Nucl Med. 1975; 16:210–224. [PubMed: 1113170]
54. Siegel S, Dahlbom M. Implementation and Evaluation of a Calculated Attenuation Correction for PET. Ieee T Nucl Sci. 1992; 39:1117–1121.
55. Chang T, Diab RH, Clark JW Jr, Mawlawi OR. Investigating the use of nonattenuation corrected PET images for the attenuation correction of PET data. Med Phys. 2013; 40:082508. [PubMed: 23927353]
56. Berker Y, Kiessling F, Schulz V. Scattered PET data for attenuation-map reconstruction in PET/MRI. Med Phys. 2014; 41:102502. [PubMed: 25281977]
57. Erdogan, H., Fessler, JA. Joint Estimation of Attenuation and Emission Images from PET Scans. Paper presented at: IEEE Nucl. Sci. Symp. Med. Im. Conf; 1999;
58. Glatting G, Wuchenauer M, Reske SN. Simultaneous iterative reconstruction for emission and attenuation images in positron emission tomography. Med Phys. 2000; 27:2065–2071. [PubMed: 11011734]

59. Salomon A, Goedicke A, Schweizer B, Aach T, Schulz V. Simultaneous reconstruction of activity and attenuation for PET/MR. IEEE Trans Med Imaging. 2011; 30:804–813. [PubMed: 21118768]
60. Rezaei A, Defrise M, Bal G, et al. Simultaneous Reconstruction of Activity and Attenuation in Time-of-Flight PET. IEEE Trans Med Imaging. 2012; 31:2224–2233. [PubMed: 22899574]
61. Defrise M, Rezaei A, Nuyts J. Time-of-flight PET data determine the attenuation sinogram up to a constant. Phys Med Biol. 2012; 57:885–899. [PubMed: 22290428]
62. Mehranian A, Zaidi H. Joint estimation of activity and attenuation in whole-body TOF PET/MRI using constrained Gaussian mixture models. IEEE Trans Med Imaging. 2015 In press.
63. Mehranian A, Zaidi H. Clinical Assessment of Emission- and Segmentation-Based MR-Guided Attenuation Correction in Whole-Body Time-of-Flight PET/MR Imaging. J Nucl Med. 2015; 56:877–883. [PubMed: 25858043]
64. Mollet P, Keereman V, Clementel E, Vandenberghe S. Simultaneous MR-compatible emission and transmission imaging for PET using time-of-flight information. IEEE Trans Med Imaging. 2012; 31:1734–1742. [PubMed: 22948340]
65. Mollet P, Keereman V, Bini J, Izquierdo-Garcia D, Fayad ZA, Vandenberghe S. Improvement of attenuation correction in time-of-flight PET/MR imaging with a positron-emitting source. J Nucl Med. 2014; 55:329–336. [PubMed: 24434291]
66. Bowen, SL., Catana, C. Transmission Imaging for a Simultaneous PET-MR System. IEEE Nucl. Sci. Symp. Conf; 2014;
67. Rothfuss H, Panin V, Moor A, et al. LSO background radiation as a transmission source using time of flight. Phys Med Biol. 2014; 59:5483–5500. [PubMed: 25163423]
68. Ouyang J, Chun SY, Petibon Y, Bonab AA, Alpert N, Fakhri GE. Bias atlases for segmentation-based PET attenuation correction using PET-CT and MR. IEEE Trans Nucl Sci. 2013; 60:3373–3382. [PubMed: 24966415]
69. Izquierdo-Garcia D, Sawiak SJ, Knesaurek K, et al. Comparison of MR-based attenuation correction and CT-based attenuation correction of whole-body PET/MR imaging. Eur J Nucl Med Mol Imaging. 2014; 41:1574–1584. [PubMed: 24652234]
70. Marshall HR, Prato FS, Deans L, Theberge J, Thompson RT, Stodilka RZ. Variable lung density consideration in attenuation correction of whole-body PET/MRI. J Nucl Med. 2012; 53:977–984. [PubMed: 22566600]
71. Jena A, Taneja S, Goel R, Renjen P, Negi P. Reliability of semiquantitative (1)(8)F-FDG PET parameters derived from simultaneous brain PET/MRI: a feasibility study. Eur J Radiol. 2014; 83:1269–1274. [PubMed: 24813529]
72. Yoon SH, Goo JM, Lee SM, Park CM, Seo HJ, Cheon GJ. Positron emission tomography/magnetic resonance imaging evaluation of lung cancer: current status and future prospects. J Thorac Imaging. 2014; 29:4–16. [PubMed: 24296699]
73. Catana C. Motion Correction Options in PET/MRI. Semin Nucl Med. 2015; 45:212–223. [PubMed: 25841276]
74. Delso G, Martinez-Moller A, Bundschuh RA, Nekolla SG, Ziegler SI. The effect of limited MR field of view in MR/PET attenuation correction. Med Phys. 2010; 37:2804–2812. [PubMed: 20632591]
75. Schramm G, Langner J, Hofheinz F, et al. Influence and compensation of truncation artifacts in MR-based attenuation correction in PET/MR. IEEE Trans Med Imaging. 2013; 32:2056–2063. [PubMed: 24186268]
76. Nuyts J, Bal G, Kehren F, Fenchel M, Michel C, Watson C. Completion of a truncated attenuation image from the attenuated PET emission data. IEEE Trans Med Imaging. 2013; 32:237–246. [PubMed: 23014717]
77. Blumhagen JO, Ladebeck R, Fenchel M, Scheffler K. MR-based field-of-view extension in MR/PET: B0 homogenization using gradient enhancement (HUGE). Magn Reson Med. 2013; 70:1047–1057. [PubMed: 23203976]
78. Blumhagen JO, Braun H, Ladebeck R, et al. Field of view extension and truncation correction for MR-based human attenuation correction in simultaneous MR/PET imaging. Med Phys. 2014; 41:022303. [PubMed: 24506641]

79. New PF, Rosen BR, Brady TJ, et al. Potential hazards and artifacts of ferromagnetic and nonferromagnetic surgical and dental materials and devices in nuclear magnetic resonance imaging. Radiology. 1983; 147:139–148. [PubMed: 6828719]
80. Kinahan PE, Hasegawa BH, Beyer T. X-ray-based attenuation correction for positron emission tomography/computed tomography scanners. Semin Nucl Med. 2003; 33:166–179. [PubMed: 12931319]
81. Ladefoged CN, Andersen FL, Keller SH, et al. PET/MR imaging of the pelvis in the presence of endoprostheses: reducing image artifacts and increasing accuracy through inpainting. Eur J Nucl Med Mol Imaging. 2013; 40:594–601. [PubMed: 23296642]
82. Bezrukov I, Schmidt H, Mantlik F, et al. MR-based attenuation correction methods for improved PET quantification in lesions within bone and susceptibility artifact regions. J Nucl Med. 2013; 54:1768–1774. [PubMed: 24009273]
83. Burger IA, Wurnig MC, Becker AS, et al. Hybrid PET/MR imaging: an algorithm to reduce metal artifacts from dental implants in Dixon-based attenuation map generation using a multiacquisition variable-resonance image combination sequence. J Nucl Med. 2015; 56:93–97. [PubMed: 25500830]
84. Lois C, Bezrukov I, Schmidt H, et al. Effect of MR contrast agents on quantitative accuracy of PET in combined whole-body PET/MR imaging. Eur J Nucl Med Mol Imaging. 2012; 39:1756–1766. [PubMed: 22890801]
85. Conti M. Why is TOF PET reconstruction a more robust method in the presence of inconsistent data? Phys Med Biol. 2011; 56:155–168. [PubMed: 21119224]
86. Davison H, ter Voert EE, de Galiza Barbosa F, Veit-Haibach P, Delso G. Incorporation of Time-of-Flight Information Reduces Metal Artifacts in Simultaneous Positron Emission Tomography/Magnetic Resonance Imaging: A Simulation Study. Invest Radiol. 2015; 50:423–429. [PubMed: 25756682]
87. Mehranian A, Zaidi H. Impact of time-of-flight PET on quantification errors in MR imaging-based attenuation correction. J Nucl Med. 2015; 56:635–641. [PubMed: 25745090]
88. Boellaard R, Hofman MB, Hoekstra OS, Lammertsma AA. Accurate PET/MR quantification using time of flight MLAA image reconstruction. Mol Imaging Biol. 2014; 16:469–477. [PubMed: 24430291]
89. Delso G, Martinez-Moller A, Bundschuh RA, et al. Evaluation of the attenuation properties of MR equipment for its use in a whole-body PET/MR scanner. Phys Med Biol. 2010; 55:4361–4374. [PubMed: 20647598]
90. Tellmann L, Quick HH, Bockisch A, Herzog H, Beyer T. The effect of MR surface coils on PET quantification in whole-body PET/MR: results from a pseudo-PET/MR phantom study. Med Phys. 2011; 38:2795–2805. [PubMed: 21776816]
91. MacDonald LR, Kohlmyer S, Liu C, Lewellen TK, Kinahan PE. Effects of MR surface coils on PET quantification. Med Phys. 2011; 38:2948–2956. [PubMed: 21815368]
92. Wollenweber SD, Delso G, Deller T, Goldhaber D, Hullner M, Veit-Haibach P. Characterization of the impact to PET quantification and image quality of an anterior array surface coil for PET/MR imaging. MAGMA. 2014; 27:149–159. [PubMed: 23800803]
93. Paulus DH, Braun H, Aklan B, Quick HH. Simultaneous PET/MR imaging: MR-based attenuation correction of local radiofrequency surface coils. Med Phys. 2012; 39:4306–4315. [PubMed: 22830764]
94. Paulus DH, Tellmann L, Quick HH. Towards improved hardware component attenuation correction in PET/MR hybrid imaging. Phys Med Biol. 2013; 58:8021–8040. [PubMed: 24168832]
95. Kartmann R, Paulus DH, Braun H, et al. Integrated PET/MR imaging: automatic attenuation correction of flexible RF coils. Med Phys. 2013; 40:082301. [PubMed: 23927344]
96. Mantlik F, Hofmann M, Werner MK, et al. The effect of patient positioning aids on PET quantification in PET/MR imaging. Eur J Nucl Med Mol Imaging. 2011; 38:920–929. [PubMed: 21308373]
97. Ferguson A, McConathy J, Su Y, Hewing D, Laforest R. Attenuation Effects of MR Headphones During Brain PET/MR Studies. J Nucl Med Technol. 2014; 42:93–100. [PubMed: 24556458]

98. Schleyer PJ, Schaeffter T, Marsden PK. The effect of inaccurate bone attenuation coefficient and segmentation on reconstructed PET images. Nucl Med Commun. 2010; 31:708–716. [PubMed: 20505553]

99. Samarin A, Burger C, Wollenweber SD, et al. PET/MR imaging of bone lesions--implications for PET quantification from imperfect attenuation correction. Eur J Nucl Med Mol Imaging. 2012; 39:1154–1160. [PubMed: 22526955]

100. Kim JH, Lee JS, Song IC, Lee DS. Comparison of Segmentation-Based Attenuation Correction Methods for PET/MRI: Evaluation of Bone and Liver Standardized Uptake Value with Oncologic PET/CT Data. J Nucl Med. 2012; 53:1878–1882. [PubMed: 23081993]

101. Akbarzadeh A, Ay MR, Ahmadian A, Alam NR, Zaidi H. MRI-guided attenuation correction in whole-body PET/MR: assessment of the effect of bone attenuation. Ann Nucl Med. 2013; 27:152–162. [PubMed: 23264064]

102. Schramm G, Langner J, Hofheinz F, et al. Quantitative accuracy of attenuation correction in the Philips Ingenuity TF whole-body PET/MR system: a direct comparison with transmission-based attenuation correction. MAGMA. 2013; 26:115–126. [PubMed: 22923020]

103. Partovi S, Kohan A, Gaeta C, et al. Image quality assessment of automatic three-segment MR attenuation correction vs. CT attenuation correction. American journal of nuclear medicine and molecular imaging. 2013; 3:291–299. [PubMed: 23638340]

104. Bini J, Izquierdo-Garcia D, Mateo J, et al. Preclinical evaluation of MR attenuation correction versus CT attenuation correction on a sequential whole-body MR/PET scanner. Invest Radiol. 2013; 48:313–322. [PubMed: 23296082]

105. Andersen FL, Ladefoged CN, Beyer T, et al. Combined PET/MR imaging in neurology: MR-based attenuation correction implies a strong spatial bias when ignoring bone. Neuroimage. 2014; 84:206–216. [PubMed: 23994317]

106. Aznar MC, Sersar R, Saabye J, et al. Whole-body PET/MRI: the effect of bone attenuation during MR-based attenuation correction in oncology imaging. Eur J Radiol. 2014; 83:1177–1183. [PubMed: 24780817]

107. Brendle C, Schmidt H, Oergel A, et al. Segmentation-based attenuation correction in positron emission tomography/magnetic resonance: erroneous tissue identification and its impact on positron emission tomography interpretation. Invest Radiol. 2015; 50:339–346. [PubMed: 25585210]

108. Dickson JC, O'Meara C, Barnes A. A comparison of CT- and MR-based attenuation correction in neurological PET. Eur J Nucl Med Mol Imaging. 2014; 41:1176–1189. [PubMed: 24425423]

109. Delso G, Carl M, Wiesinger F, et al. Anatomic evaluation of 3-dimensional ultrashort-echo-time bone maps for PET/MR attenuation correction. J Nucl Med. 2014; 55:780–785. [PubMed: 24639457]

110. Arabi H, Rager O, Alem A, Varoquaux A, Becker M, Zaidi H. Clinical Assessment of MR-Guided 3-Class and 4-Class Attenuation Correction in PET/MR. Mol Imaging Biol. 2015; 17:264–276. [PubMed: 25096328]

111. Keller SH, Holm S, Hansen AE, et al. Image artifacts from MR-based attenuation correction in clinical, whole-body PET/MRI. MAGMA. 2013; 26:173–181. [PubMed: 22996323]

112. Eiber M, Martinez-Moller A, Souvatzoglou M, et al. Value of a Dixon-based MR/PET attenuation correction sequence for the localization and evaluation of PET-positive lesions. Eur J Nucl Med Mol Imaging. 2011; 38:1691–1701. [PubMed: 21688050]

113. Drzezga A, Souvatzoglou M, Eiber M, et al. First clinical experience with integrated whole-body PET/MR: comparison to PET/CT in patients with oncologic diagnoses. J Nucl Med. 2012; 53:845–855. [PubMed: 22534830]

114. Fraum TJ, Fowler KJ, McConathy J, et al. PET/MRI for the body imager: abdominal and pelvic oncologic applications. Abdom Imaging. 2015

115. Schafer JF, Gatidis S, Schmidt H, et al. Simultaneous whole-body PET/MR imaging in comparison to PET/CT in pediatric oncology: initial results. Radiology. 2014; 273:220–231. [PubMed: 24877983]

116. Jeong JH, Cho IH, Kong EJ, Chun KA. Evaluation of Dixon Sequence on Hybrid PET/MR Compared with Contrast-Enhanced PET/CT for PET-Positive Lesions. Nucl Med Mol Imaging. 2014; 48:26–32. [PubMed: 24900135]

117. Hitz S, Habekost C, Furst S, et al. Systematic Comparison of the Performance of Integrated Whole-Body PET/MR Imaging to Conventional PET/CT for 18F-FDG Brain Imaging in Patients Examined for Suspected Dementia. J Nucl Med. 2014; 55:923–931. [PubMed: 24833495]

118. Varoquaux A, Rager O, Poncet A, et al. Detection and quantification of focal uptake in head and neck tumours: (18)F-FDG PET/MR versus PET/CT. Eur J Nucl Med Mol Imaging. 2014; 41:462–475. [PubMed: 24108458]

119. Kohan AA, Kolthammer JA, Vercher-Conejero JL, et al. N staging of lung cancer patients with PET/MRI using a three-segment model attenuation correction algorithm: initial experience. Eur Radiol. 2013; 23:3161–3169. [PubMed: 23765261]

Key Points

- Accurate attenuation correction (AC) is required to avoid biasing PET image quantification.
- PET/MR attenuation correction (MR-AC) methods aim to provide accurate AC using the information provided from the PET and/or MR images in combined PET/MR scanners.
- MR-AC methods are divided into segmentation-based, atlas-based and PET-based approaches, each with its own pros and cons.
- Whole body imaging remains especially challenging and further efforts need to concentrate on this area in the future.
- Metallic implants, body truncation, hardware correction, motion, high inter- and intra-subject variability for lung density are some of the major challenges that future MR-AC approaches would be required to face.

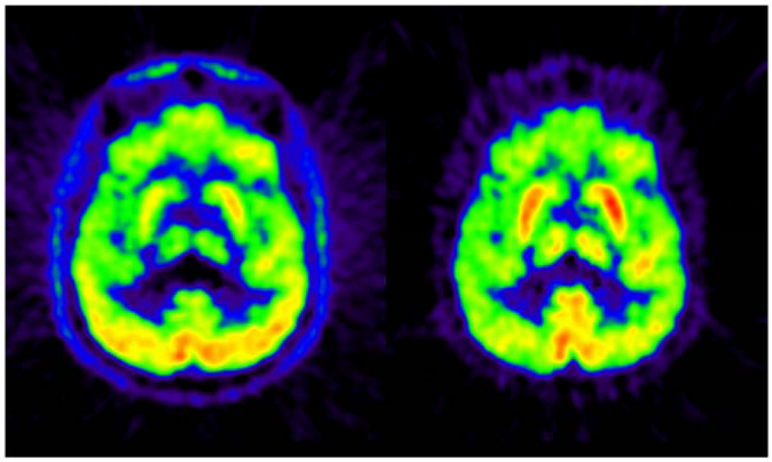

Fig. 1.
PET images reconstructed without (left) and with (right) AC. Note the attenuation effect producing larger reduction of activity towards the center of the head.

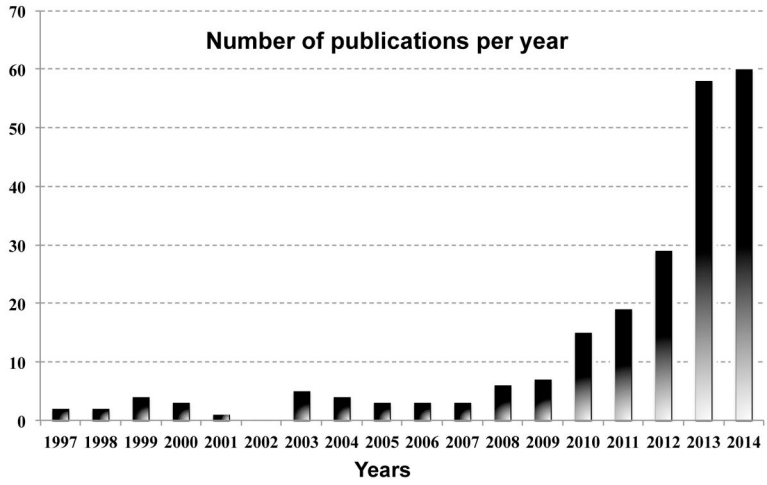

Fig. 2.
PubMed results on search “PET and MR and attenuation correction”. Source: PubMed.

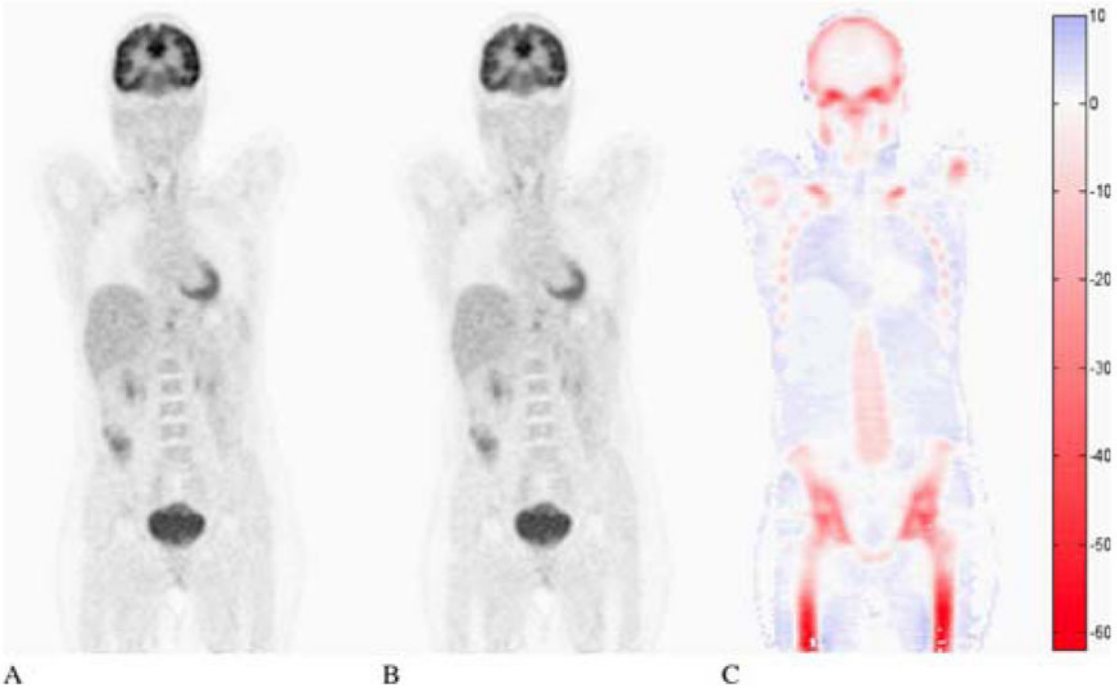

Fig. 3.

Image quantification bias when bone is not taken into account: PET image reconstructed with CT-AC (A) or with the same CT-AC but with all bone structures set to the attenuation value of soft tissue (B) and relative differences in percentage (C). Figure originally from Hofmann, M., et al. (2009). “Towards quantitative PET/MRI: a review of MR-based attenuation correction techniques.” Eur J Nucl Med Mol Imaging 36 Suppl 1: S93–104.

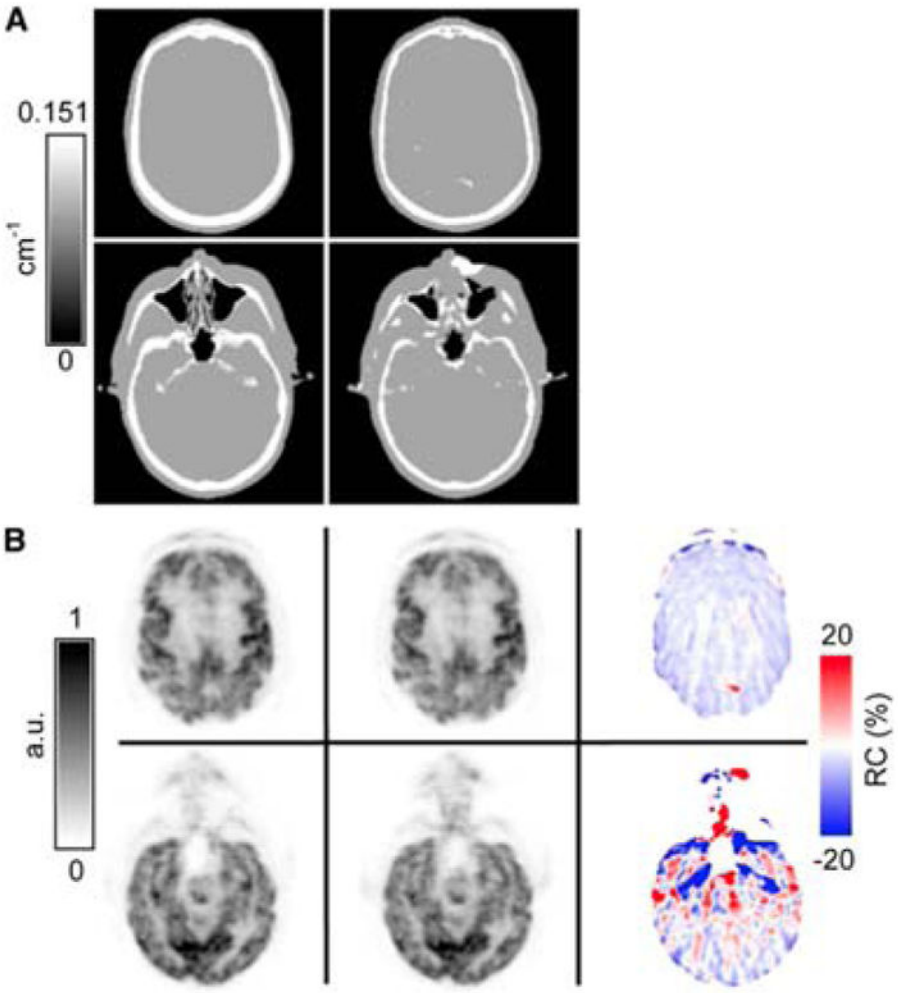

Fig. 4.

Use of UTE sequence for MR-AC application: (A) μ-maps for segmented CT-AC (left) and UTE-based MR-AC (right); (B) Reconstructed PET images using CT-AC (left) and UTE-based MR-AC (middle) and their relative differences (right). This research was originally published in *JNM*. From Catana, C., et al. (2010). "Toward implementing an MRI-based PET attenuation-correction method for neurologic studies on the MR-PET brain prototype." J Nucl Med 51(9): 1431–1438. © by the Society of Nuclear Medicine and Molecular Imaging, Inc.

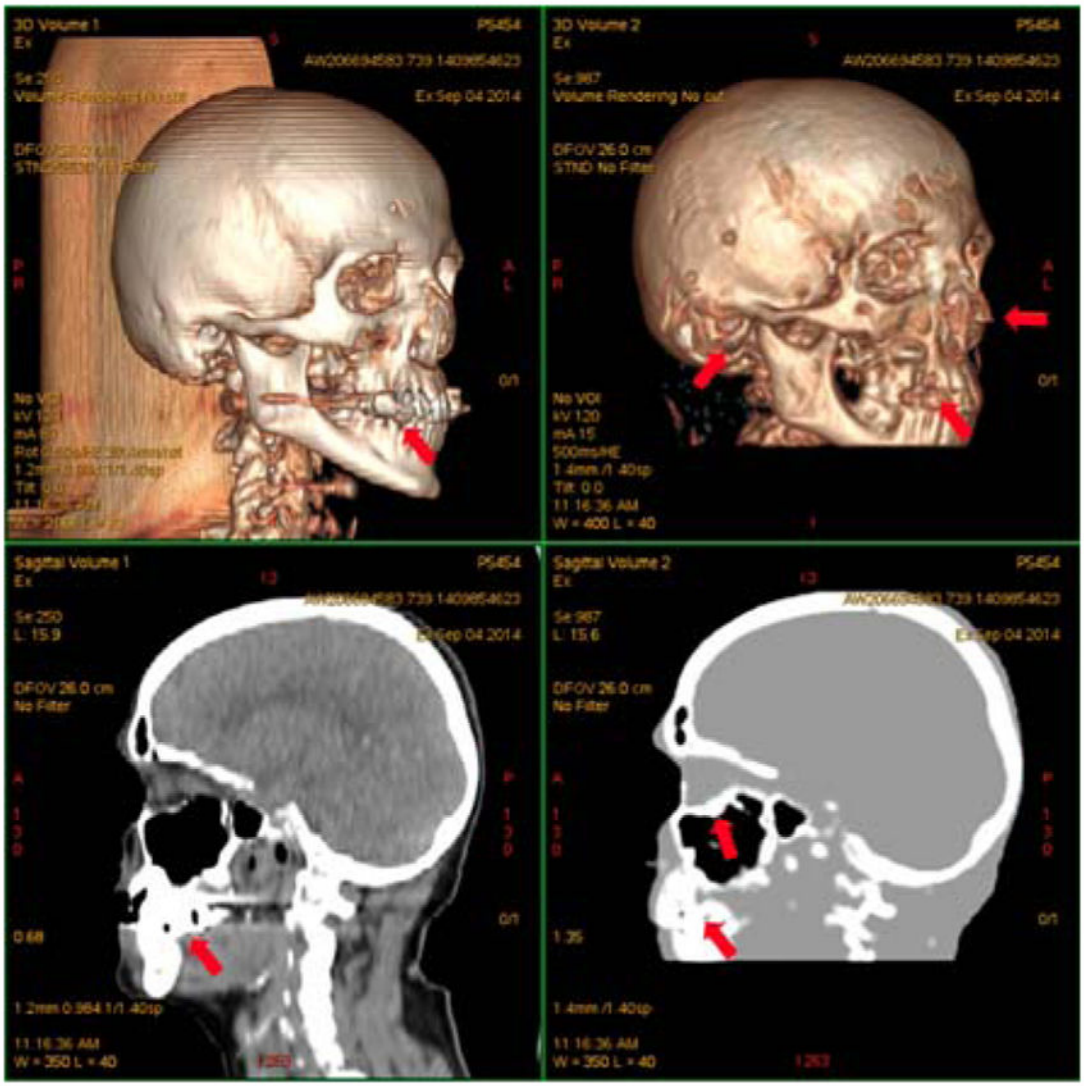

Fig. 5.

Segmentation results obtained with a ZT sequence (right) and its comparison with a CT image (left). Arrows point to dental artifacts, minor misclassification of cartilage and auditory canal air and oversegmentation on the sinuses. This research was originally published in *JNM*. Delso, G., et al. (2015). “Clinical Evaluation of Zero-Echo-Time MR Imaging for the Segmentation of the Skull.” J Nucl Med 56(3): 417–422. © by the Society of Nuclear Medicine and Molecular Imaging, Inc.

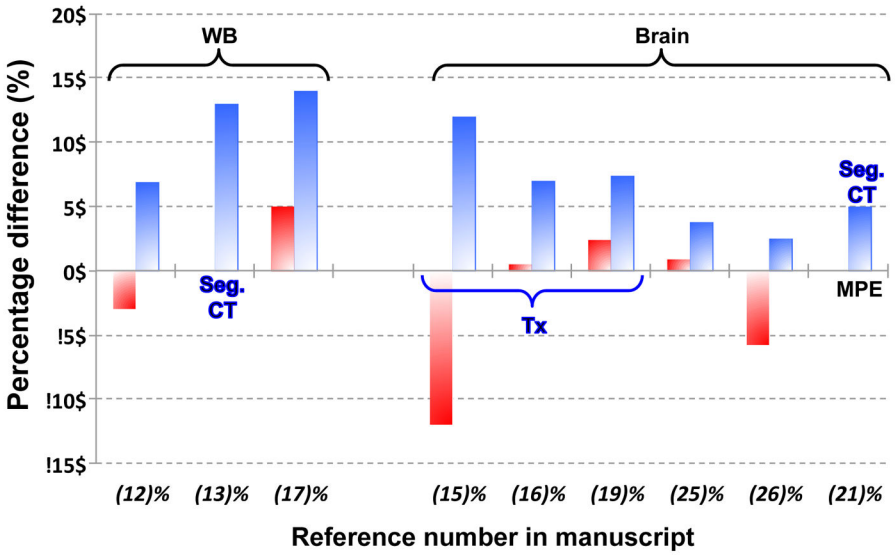

Fig. 6.

Comparison of Minimum (red) and Maximum (blue) Percentage differences of PET reconstructed images versus the gold-standard, CT-AC, unless explicitly written otherwise: Tx = Transmission-based AC; Seg. CT = Segmented CT AC. Where available MPE = Mean Percentage Error replaces maximum percentage differences. Figures taken from literature where specific concrete values were available.

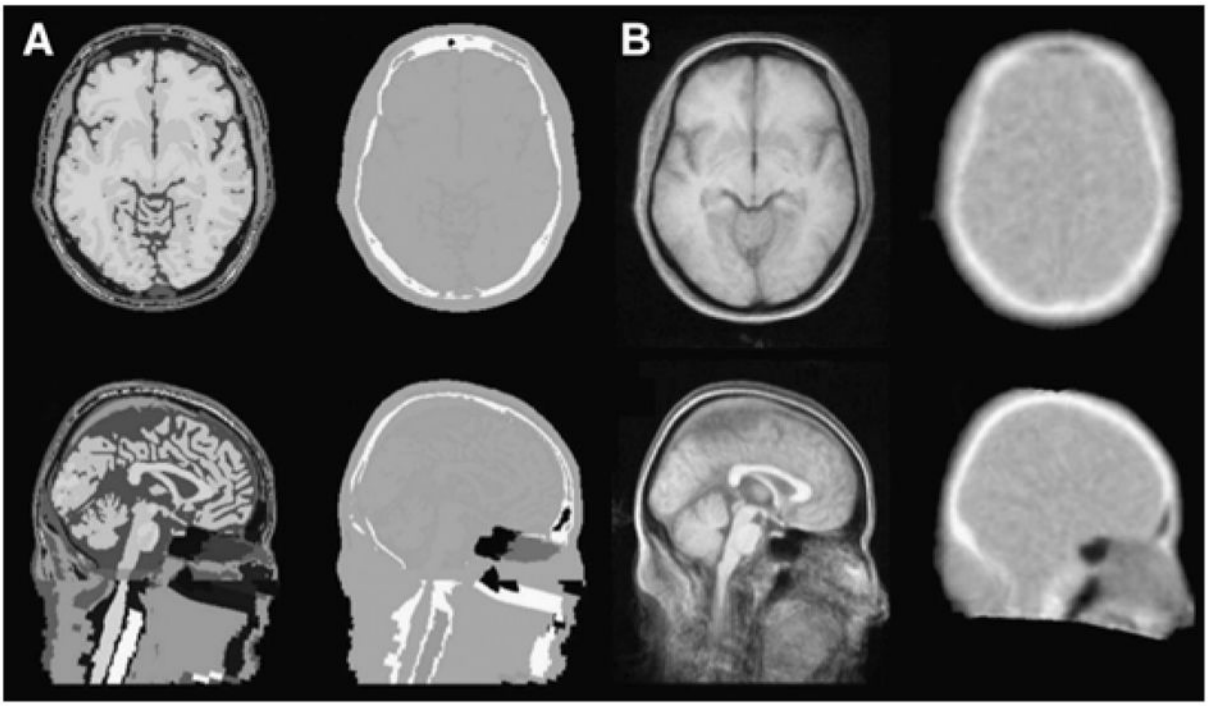

Fig. 7.

Axial (top row) and sagittal (bottom row) slices for MRI and attenuation maps for a tissue atlas (A) and a template created using vtkCISG (B). This research was originally published in *JNM*. Malone, I. B., et al. (2011). “Attenuation correction methods suitable for brain imaging with a PET/MRI scanner: a comparison of tissue atlas and template attenuation map approaches.” J Nucl Med 52(7): 1142–1149. © by the Society of Nuclear Medicine and Molecular Imaging, Inc.

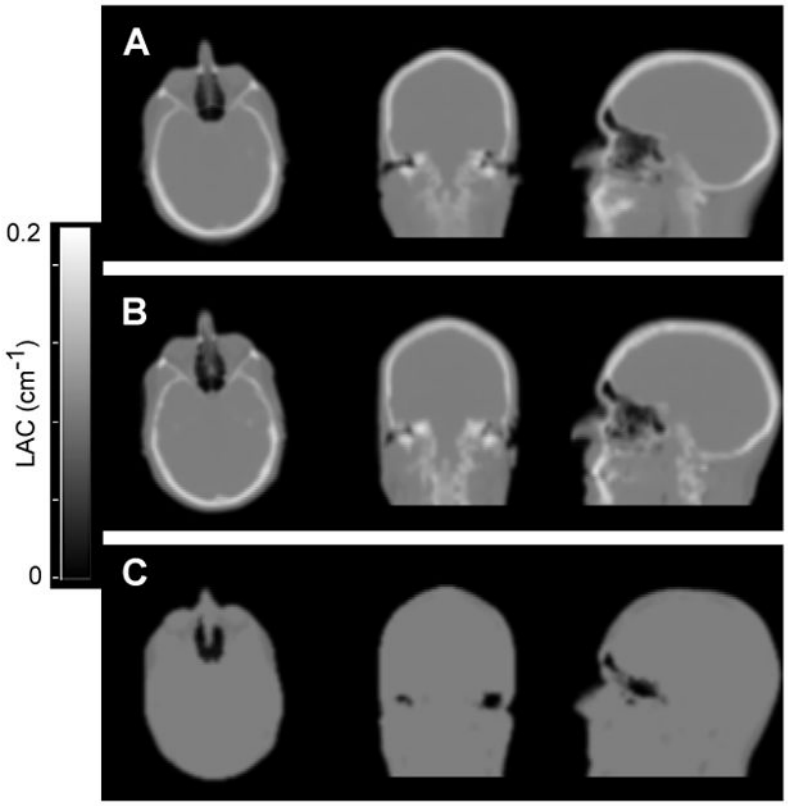

Fig. 8.

Comparison of attenuation maps from new SPM8 atlas method (A); from CT (B) and from Dixon-based method (C). This research was originally published in *JNM*. Izquierdo-Garcia, D., et al. (2014). “An SPM8-based approach for attenuation correction combining segmentation and nonrigid template formation: application to simultaneous PET/MR brain imaging.” J Nucl Med 55(11): 1825–1830. © by the Society of Nuclear Medicine and Molecular Imaging, Inc.

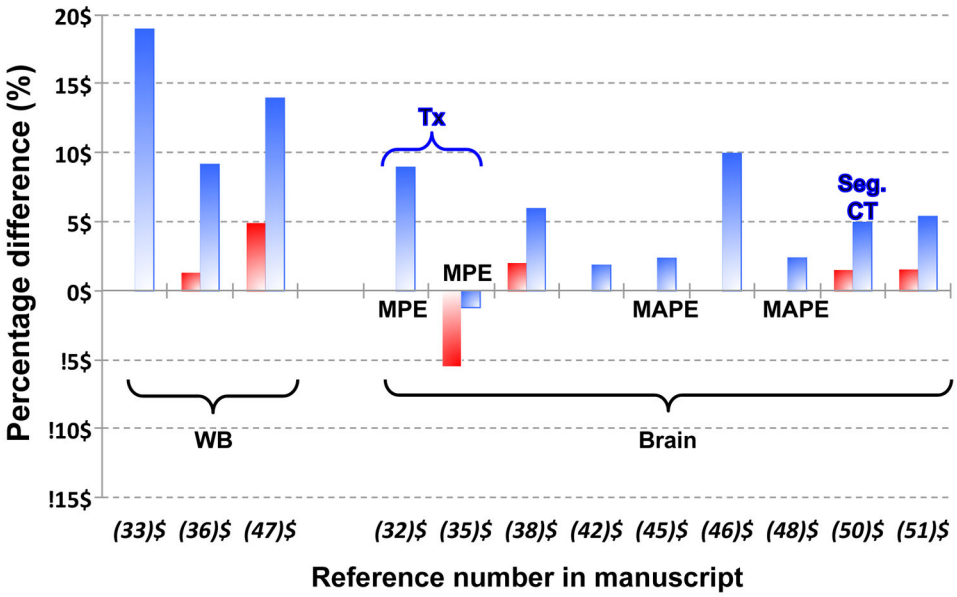

Fig. 9.

Comparison of Minimum (red) and Maximum (blue) Percentage differences of PET reconstructed images versus the gold-standard, CT-AC, unless explicitly written otherwise: Tx = Transmission-based AC; Seg. CT = Segmented CT-AC. Where available: MPE = Mean Percentage Error or MAPE = Mean Absolute Percentage Error, replaces maximum percentage differences. Figures taken from literature where specific concrete values were available.

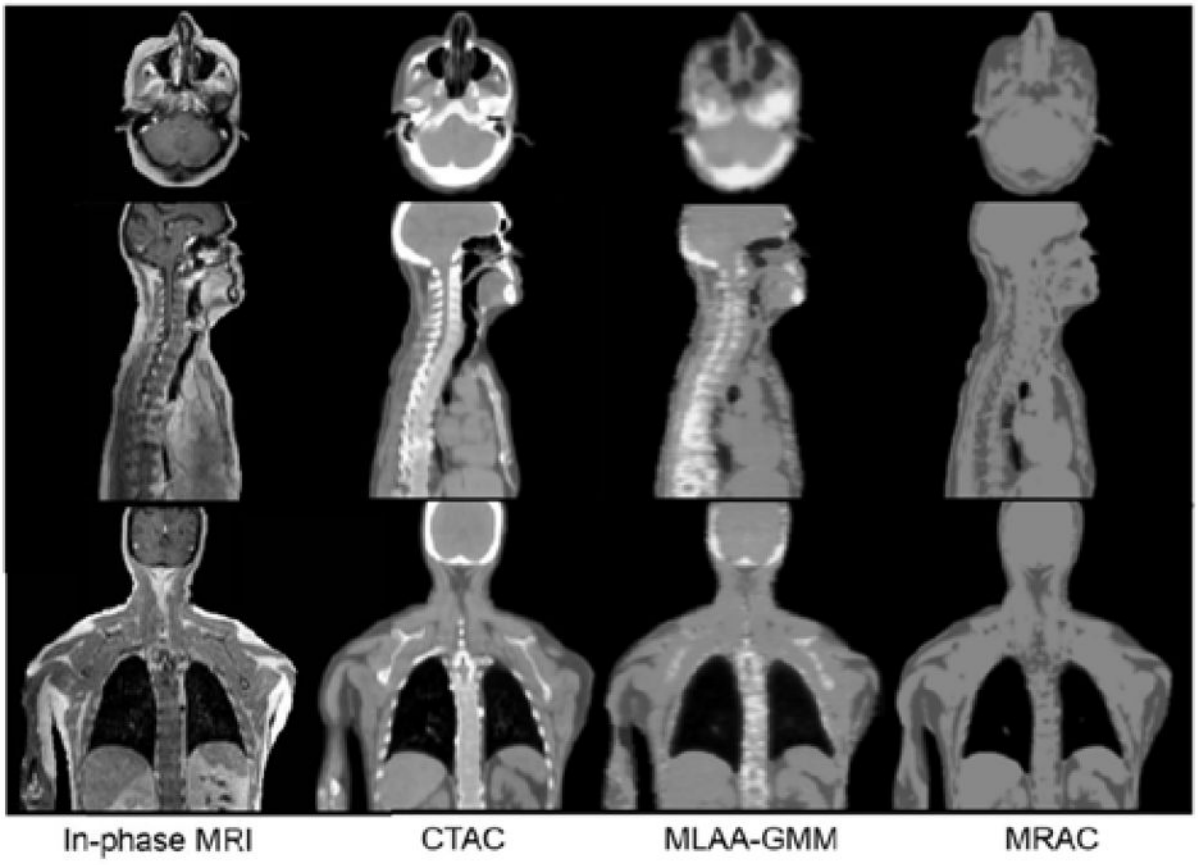

Fig. 10.

Comparison of mu-maps using MLAA-GMM method, the standard 4-class segment MR-AC method and their reference CT-AC. This research was originally published in *JNM*. Mehranian, A. and H. Zaidi (2015). “Clinical assessment of emission- and segmentation-based MRI-guided attenuation correction in whole-body TOF PET/MRI.” J Nucl Med. Apr. 9. Epub ahead of print. © by the Society of Nuclear Medicine and Molecular Imaging, Inc.

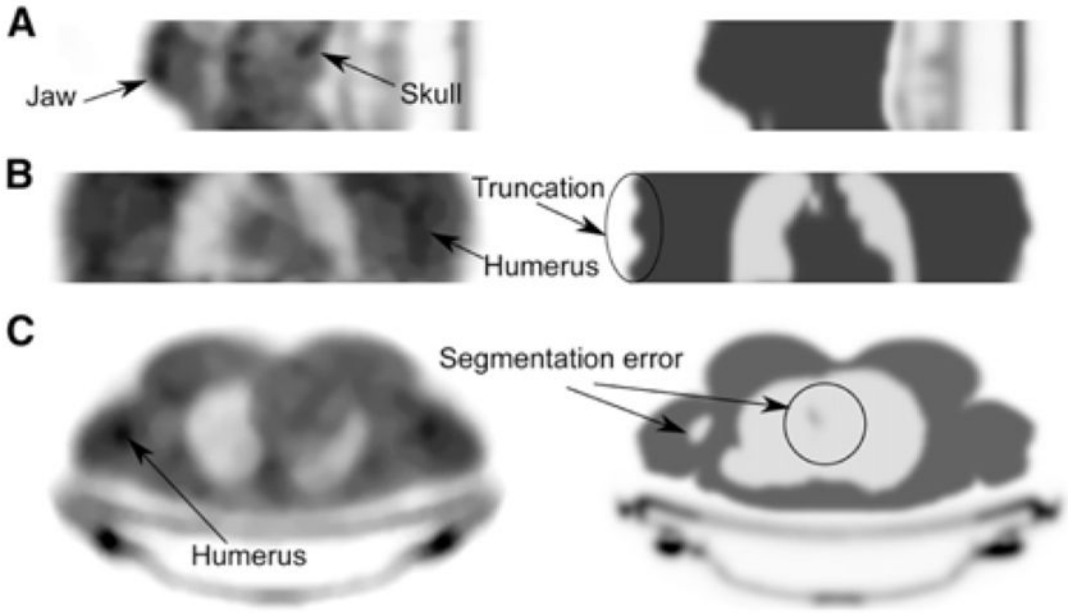

Fig. 11.

Comparison of transmission-based (left) vs. segmentation-based MR-AC (right) on 3 subjects: for head and neck (A); torso in coronal view (B) and torso in axial view (C). This research was originally published in *JNM*. Mollet, P., et al. (2014). “Improvement of attenuation correction in time-of-flight PET/MR imaging with a positron-emitting source.” J Nucl Med 55(2): 329–336. © by the Society of Nuclear Medicine and Molecular Imaging, Inc.

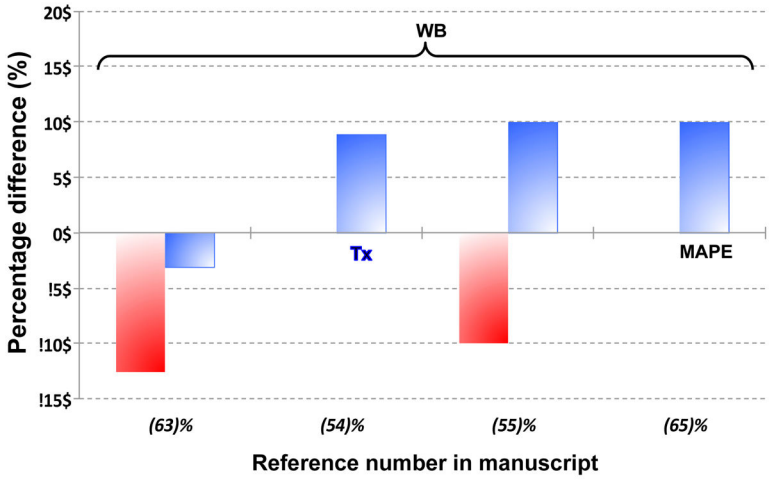

Fig. 12.

Comparison of Minimum (red) and Maximum (blue) Percentage differences of PET reconstructed images versus the gold-standard, CT-AC, unless explicitly written otherwise: Tx = Transmission-based AC. Where available: MAPE = Mean Absolute Percentage Error, replaces maximum percentage differences. Figures taken from literature where specific concrete values were available.

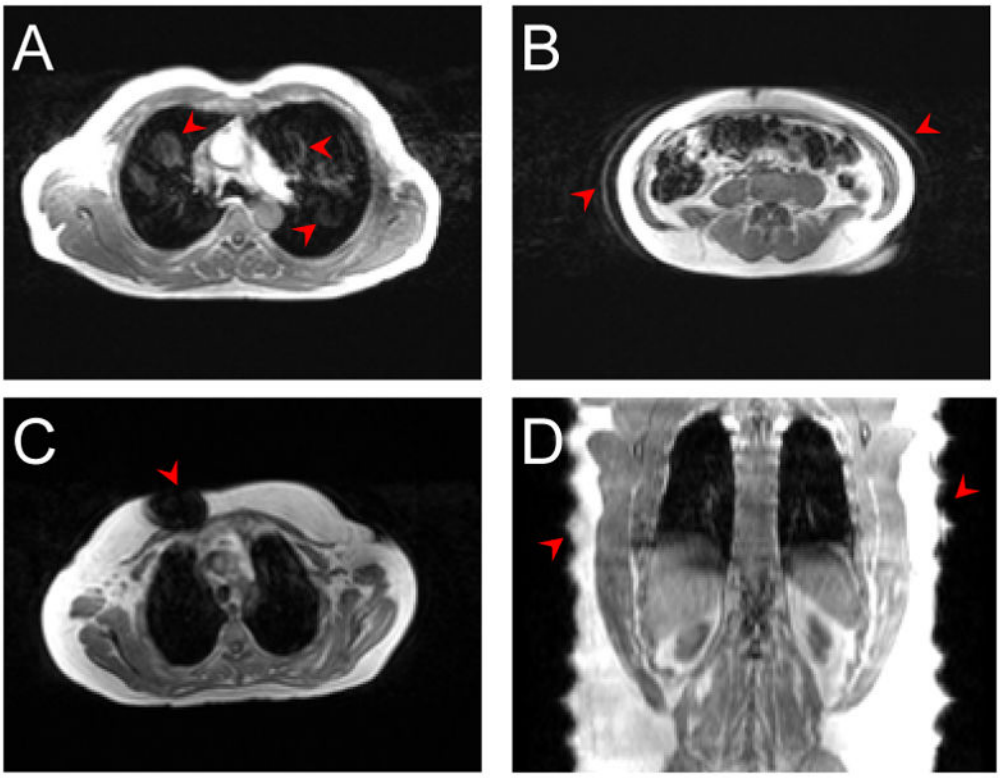

Fig. 13.

Examples of common MR artifacts that impact the quality of MR-AC approaches: flow (A) and respiratory motion artifacts (B), metallic implant (C) and body truncation artifacts due to limited FoV (D). Figure originally from Izquierdo-Garcia, D., et al. (2014). “Comparison of MR-based attenuation correction and CT-based attenuation correction of whole-body PET/MR imaging.” Eur J Nucl Med Mol Imaging 41(8): 1574–1584.

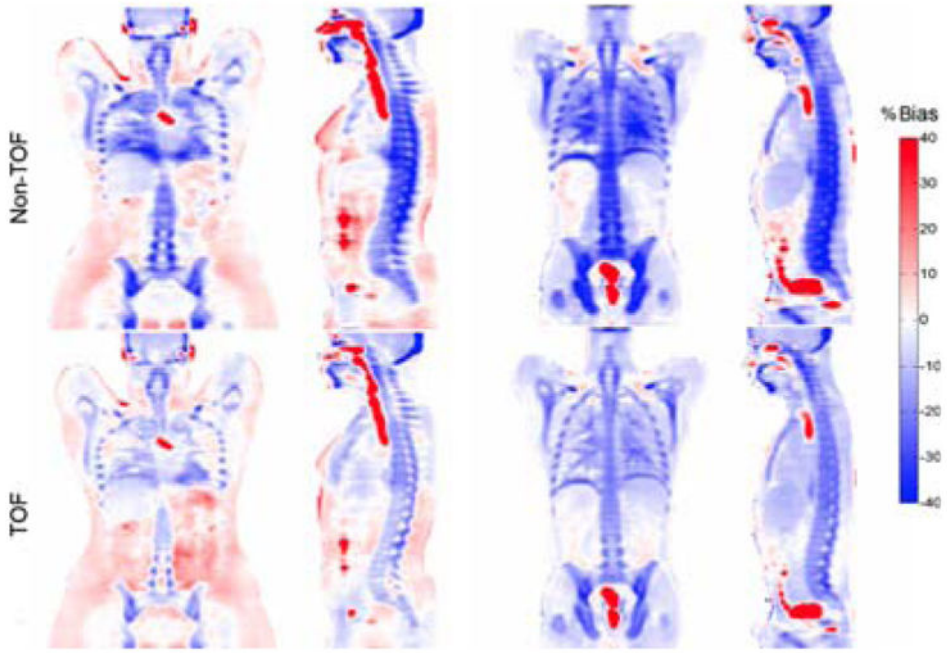

Fig. 14.

Comparison of bias between the standard 4-class segmentation MR-AC approach and CT-AC with non-ToF (top row) and ToF (bottom row) capabilities. This research was originally published in *JNM*. Mehranian, A. and H. Zaidi (2015). “Impact of Time-of-Flight PET on Quantification Errors in MR Imaging-Based Attenuation Correction.” J Nucl Med 56(4): 635–641. © by the Society of Nuclear Medicine and Molecular Imaging, Inc.

Table 1

Summary of the Pros and Cons of the MR-AC Segmentation-based approaches

✓ **Pros**	✗ **Cons**
✓ Easy implementation	✗ Robustness (noise, bias,...)
✓ Low computational cost	✗ Bone/Air segmentation
✓ Whole-Body applicability	✗ Discrete LACs

Table 2

Summary of the Pros and Cons of the Atlas-based MR-AC approaches

✓ **Pros**	✗ **Cons**
✓ Robustness (noise, bias,...)	✗ Subject-specific variability
✓ Bone identification	✗ Whole-body
✓ Continuous LACs	✗ Computational cost

Table 3

Summary of the Pros and Cons of the PET-AC approaches

✓ **Pros**	✗ **Cons**
✓ MR time for clinical use	✗ Cross-Talk and emission data in all LORs (Joint-based)
✓ Robust to artifacts	✗ Computational cost (Joint-based)
✓ Implants body truncation, hardware attenuation	✗ Extended acquisition time (Tx)
✓ Whole-Body applicability	✗ Noise + additional radiation (Tx)
	✗ Accuracy (emission-based)